

# SCIENTIFIC REPORTS



OPEN

## Deciphering the relationship among phosphate dynamics, electron-dense body and lipid accumulation in the green alga *Parachlorella kessleri*

Received: 16 December 2015

Accepted: 18 April 2016

Published: 16 May 2016

Shuhei Ota<sup>1,2</sup>, Mai Yoshihara<sup>1</sup>, Tomokazu Yamazaki<sup>1,2</sup>, Tsuyoshi Takeshita<sup>1</sup>, Aiko Hirata<sup>3</sup>, Mami Konomi<sup>4</sup>, Kenshiro Oshima<sup>5</sup>, Masahira Hattori<sup>5</sup>, Kateřina Bišová<sup>6</sup>, Vilém Zachleder<sup>6</sup> & Shigeyuki Kawano<sup>1,2</sup>

Phosphorus is an essential element for life on earth and is also important for modern agriculture, which is dependent on inorganic fertilizers from phosphate rock. Polyphosphate is a biological polymer of phosphate residues, which is accumulated in organisms during the biological wastewater treatment process to enhance biological phosphorus removal. Here, we investigated the relationship between polyphosphate accumulation and electron-dense bodies in the green alga *Parachlorella kessleri*. Under sulfur-depleted conditions, in which some symporter genes were upregulated, while others were downregulated, total phosphate accumulation increased in the early stage of culture compared to that under sulfur-replete conditions. The P signal was detected only in dense bodies by energy dispersive X-ray analysis. Transmission electron microscopy revealed marked ultrastructural variations in dense bodies with and without polyphosphate. Our findings suggest that the dense body is a site of polyphosphate accumulation, and *P. kessleri* has potential as a phosphate-accumulating organism.

Phosphorus (P) is a non-renewable resource and is an essential element for life on earth, as well as for modern food production. Applications of inorganic fertilizers were expanded after the 1950s, and approximately 17.6 Mt of P were extracted worldwide from finite phosphate rock for conversion to fertilizers in 2009<sup>1,2</sup>. Several studies have reported that maximum phosphorus production could be reached in the near future. Cordell and White<sup>3</sup> reviewed literature on the scarcity of global phosphorus and sustainable future pathways and discussed key issues for global phosphorus security. Eutrophication of surface water in aquatic ecosystems is another phosphate-related environmental issue. Some studies have focused on phosphorus removal in waste stabilization ponds<sup>4,5</sup>. Some algae can store phosphate (Pi) through luxury uptake of Pi, and the Pi enriched biomass has a potential for using as algae-based bio-fertilizer<sup>6</sup>.

Poly-P is a biological polymer composed of inorganic phosphate (Pi) residues linked by “high-energy” phosphoanhydride bonds<sup>7,8</sup>. Poly-P has a wide range of regulatory functions, including roles as energy and inorganic phosphate reservoirs<sup>7,8</sup>, and is found in prokaryotes<sup>9–11</sup>, eukaryotes<sup>12–17</sup>, and unicellular algae, such as *Cyanidioschyzon merolae*<sup>18,19</sup>, *Chlamydomonas reinhardtii*<sup>20,21</sup>, and *Chlorella* species<sup>22,23</sup>. The well-known fluorescent label for nucleic acids, 4',6-diamidino-2-phenylindole (DAPI), interacts with poly-P at high concentrations to form DAPI-poly-P complexes that allow poly-P-rich granules to be visualized by fluorescence microscopy at

<sup>1</sup>Department of Integrated Biosciences, Graduate School of Frontier Sciences, University of Tokyo, Kashiwa, Chiba, 277-8562, Japan. <sup>2</sup>CREST, Japan Science and Technology Agency, Tokyo, Japan. <sup>3</sup>Bioimaging Center, Graduate School of Frontier Science, University of Tokyo, Kashiwa, Chiba, 277-8562, Japan. <sup>4</sup>Hitachi High-Technologies Corporation, Science & Medical Systems Business Group, Nishi-shinbashi, Tokyo, 105-8717, Japan. <sup>5</sup>Center for Omics and Bioinformatics, Graduate School of Frontier Sciences, University of Tokyo, Kashiwa, Chiba, 277-8561, Japan. <sup>6</sup>Institute of Microbiology, CAS, Centre Algatech, Laboratory of Cell Cycles of Algae, Třeboň, Czech Republic. Correspondence and requests for materials should be addressed to S.K. (email: kawano@k.u-tokyo.ac.jp)

an emission wavelength of 475–525 nm<sup>24</sup>, which produces a yellowish color. This DAPI-staining method is commonly used to detect poly-P-rich organelles *in vivo* and *in vitro*<sup>16,25,26</sup>.

Macronutrient (nitrogen, phosphate, and sulfur) limitation is a trigger for enhancing lipid accumulation in microalgae<sup>27</sup>. Some studies have used nitrogen deprivation, while others have focused on sulfur (S) deprivation, which can induce starch accumulation<sup>27,28</sup>. The relationship between nutrient limitation and polyphosphate accumulation has been the subject of several reports<sup>15,21,29,30</sup>. However, the relationship between sulfur deprivation and polyphosphate accumulation remains unclear. In this study, we revealed the relationship between DBs and poly-P dynamics under sulfur-deficient conditions in *Parachlorella kessleri*. *P. kessleri*, formerly known as *Chlorella kessleri*, is a freshwater green microalga in the family Chlorellaceae and class Trebouxiophyceae<sup>31</sup>. Because algal biomass and lipid studies have been performed on *P. kessleri*, it is a representative species for research into algal biofuel and biomass applications<sup>27,32–34</sup>. Although the association between lipid accumulation and S-deficiency has been reported<sup>32,33</sup>, the relationship between Pi dynamics and nutrient limitation remains unknown, and the site of poly-P accumulation in S-depleted *Chlorella* cells is also unclear.

To address this question, we examined the time course of total phosphate (total-P) and poly-P accumulation under S- and P-depleted conditions. Furthermore, we analyzed the ultrastructure and volumetric dynamics of S-depleted cells by transmission electron microscopy (TEM) and three-dimensional (3D)-TEM. To reveal the elemental profiles and P contents of the DB as well as non-DB regions, we performed EDX analysis using a scanning transmission electron microscope (STEM). Finally, to examine the transcriptomic responses of genes related to S metabolism, such as phosphate transporters and copper transporters/chaperones, we re-analyzed RNA-Seq data<sup>35</sup> of 2-day-old cells cultured under S-depleted and -replete conditions.

## Results

**DAPI staining of poly-P in S-depleted *P. kessleri* cells.** DIC and fluorescent microscopy revealed that DAPI-stained poly-P granules were evident in *P. kessleri* cells cultured under S-depleted conditions or in S-deficient medium (Fig. 1a,b, Fig. S1). Numerous yellowish granules were observed using fluorescence microscopy (Fig. 1b). The poly-P granules with high-fluorescence (Fig. 1, arrows) resembled the distribution of the DBs in terms of their shape and position (Fig. 1c); however, some multiple poorly defined ‘blurred’ areas were also observed (Fig. 1, arrowhead), of which identical structure was not clear in TEM. Under S-depleted conditions, DBs accumulated concomitantly with lipid bodies (Fig. 1c). The DBs were conspicuous, and varied in size and position. Large DBs were frequently located at the cell periphery (Fig. 1c).

To assess the chemical composition of the DBs, we used the following three staining methods; uranyl acetate-lead citrate<sup>36</sup>, periodic acid-thiocarbohydrazide silver proteinate (PAS), and no staining (Fig. 1d–f). PAS stains starch and sugars<sup>37</sup>. The electron density of triple serial sections derived from the same cell can be compared using these staining methods. Following staining with uranyl acetate and lead citrate, the DBs were highly electron-opaque (Fig. 1d), whereas they were negatively stained with PAS (Fig. 1e). A non-stained section exhibited relatively electron-opaque DBs (Fig. 1f), indicating that the DBs have affinity for osmium tetroxide (OsO<sub>4</sub>). As expected, starch grains were strongly PAS-stained (Fig. 1e), and lipid bodies had high affinity for OsO<sub>4</sub> (Fig. 1f). Therefore, the DBs contained organic compounds other than sugars and lipids.

**Lipid and P accumulation are accelerated under S-depleted conditions.** To eliminate any influence of the light–dark cycle on Pi accumulation, cultures were irradiated with continuous light in the present assay. In nutrient-replete Tris-acetate-phosphate (TAP) medium, exponential growth was observed in 1-day-old batch cultures, and the culture reached stationary phase after 7 d (Fig. 2a). In the S-depleted (dSTAP) and P-depleted (dPTAP) cultures, growth was repressed compared to that in TAP culture (Fig. 2a), but growth in dSTAP was compromised to a greater degree (Fig. 2a). No clear stationary phase was evident in the dSTAP culture: the number of cells increased gradually beginning at day 1 through the end of the culture period (Fig. S2). Hereinafter, 0–2 d, 3–6 d, and >7 d of culture are referred to as the early, middle, and late stages of culture, respectively.

We monitored the time-course of total lipid content during batch culture (Fig. 2b). Under S-depleted conditions, the lipid content increased from the initial day and peaked at 6 d (Fig. 2b). Thereafter, the lipid level in the dSTAP culture decreased gradually. In the dPTAP culture, total lipid levels were slightly higher than those under TAP culture in the middle and late stages (Fig. 2b).

To elucidate the P dynamics during batch culture, we determined incorporated total-P levels using a molybdenum-blue assay (Fig. 2c). After the transfer of cells to dSTAP medium, the total-P amount increased rapidly from day 0, plateaued at 2 d, and then decreased slightly after 4 d. In the TAP culture, total-P levels peaked at 1 d, then decreased from 1 to 2 d, and remained stable thereafter. At the end of the batch (9-day-old culture), 79.9% and 95.5% of phosphate still remained in media of the TAP and dSTAP, respectively (Fig. S3), indicating that phosphate is not a limiting factor for the growth. In dPTAP culture, the total-P level decreased from 0 to 2 d, and was absent thereafter (Fig. 2c).

We also examined the time-course of poly-P levels (Fig. 2d). In the dSTAP culture, poly-P accumulated rapidly from 0 to 1 d, and a high concentration was maintained from 1 to 3 d. Total-P accumulation was fivefold greater than that in TAP culture at 2 d, and almost half of the Pi had accumulated as incorporated poly-P at this time point. After 3 d, the amount of poly-P decreased rapidly, and did not change after 4 d. Although a slight peak in poly-P levels in the TAP culture at day 1 was observed, no differences were observed between the TAP and the dPTAP cultures in the middle and late stages.

**3D-TEM and volumetric dynamics of DB and lipid bodies.** To investigate the ultrastructure and volumetric dynamics of the cells in the middle stage of culture, we conducted a serial-section-based 3D-TEM analysis. We compared 3D-structures of zero-control, starch cells (starch-containing cells), and lipid cells (lipid-containing cells) in the middle stage of culture. The zero-control cell represents a 4-day-old culture under nutrient-replete

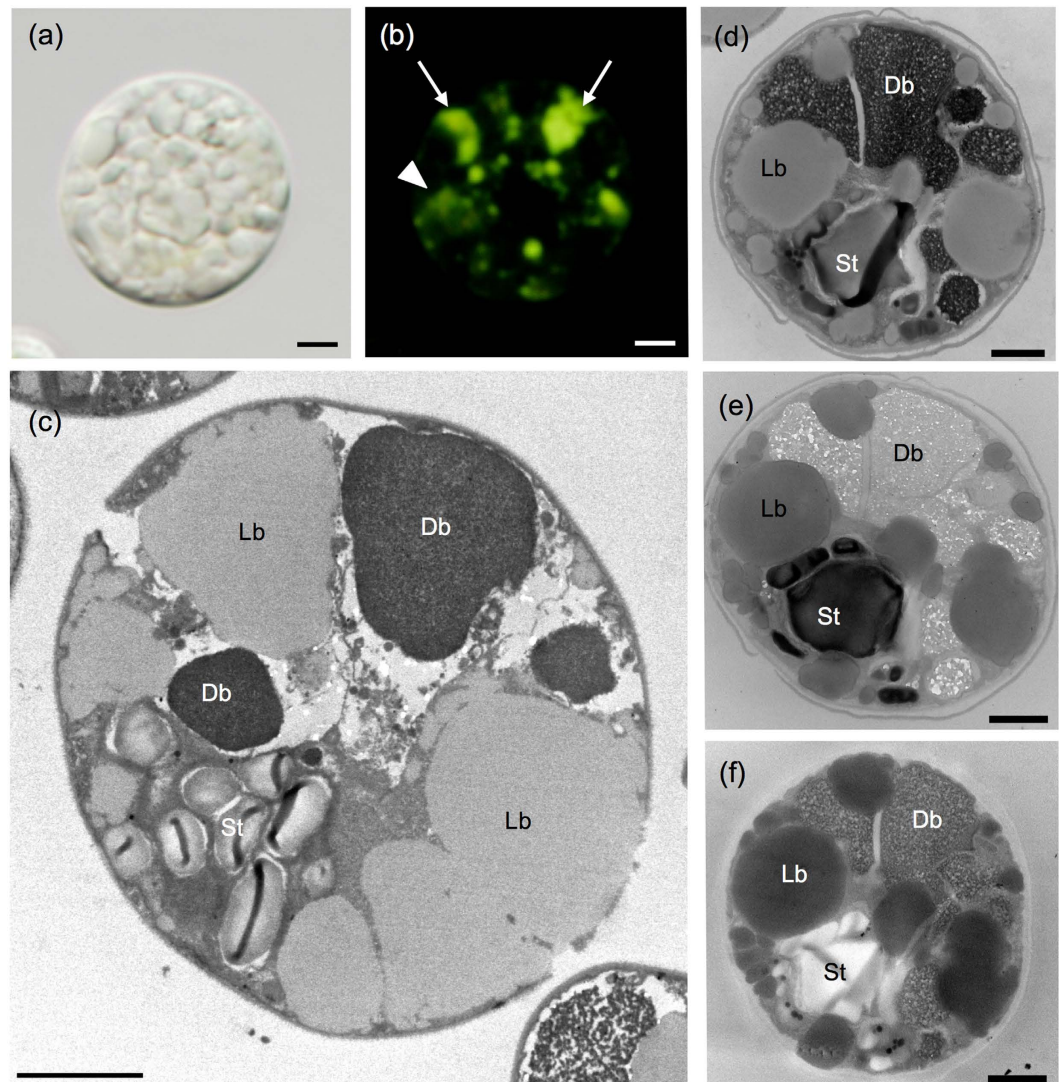


**Figure 1. DAPI–poly-P and DBs under S-depleted conditions.** Differential interference contrast image (a) and fluorescent image (b) of a DAPI-stained cell from a 6-day-old culture. (Arrows: the poly-P granules with high-fluorescence; arrowhead: blurred area of the poly-P signals) Yellow fluorescent granules indicate sites of poly-P accumulation. (c) General ultrastructure of a cell from a 6-day-old culture accumulating DBs and lipid bodies. (d–f) Triple serial sections derived from a single cell from a 5-day-old culture and subjected to the following staining methods: uranyl acetate and lead citrate staining (d), periodic acid-thiocarbohydrazide-silver proteinate (PAS) staining (e), and no staining (f). Db: electron-dense body, Lb: lipid body, St: starch. Bars = 2  $\mu$ m (a–c); 1  $\mu$ m (d–f).

conditions (stress-free conditions), which is same culture age as the pre-culture. Starch and lipid cells correspond 6-day-old cell grown in S-deficient medium (dSTAP) under a 12:12h light:dark photoperiod (starch cell), or under continuous light (LL) (lipid cell).

In the zero-control cell, a cup-shaped chloroplast was evident, and neither lipid bodies nor starch granules were observed (Fig. 3a,b; see also Movies S1–S3). The DBs were small granules localized in vacuoles (Fig. 3c). Based on the 3D-TEM volumetric analysis, the volume of the chloroplast and DBs of the zero-control cell contributed 40.7 and 1.1%, respectively, to the total cell volume.

In the starch cell, many starch grains and few lipid bodies were observed (Fig. 3d,e; see also Movies S4–S6). In this cell, the DBs were larger than those in the zero-control cell (Fig. 3f). Based on the volumetric analysis, the volumes of the chloroplast, DBs and lipids contributed 35.8, 8.1, and 0.4%, respectively, to the total cell volume.

The lipid cell exhibited a highly conspicuous degenerated chloroplast at the cell periphery, and concomitant hyper-accumulation of lipids was observed (Fig. 3g,h; see also Movies S7–S10). At this stage, fewer DBs were present but were well developed and conspicuous in the vacuoles (Fig. 3i). Based on the volumetric analysis, the volumes of the chloroplast, DBs, and lipids contributed 4.6, 12.4, and 50.4%, respectively, to the total cell volume. The 3D-TEM data indicate that lipid hyper-accumulation co-occurs with DB accumulation and that the continuous-light conditions enhanced the effect of sulfur deficiency stress.

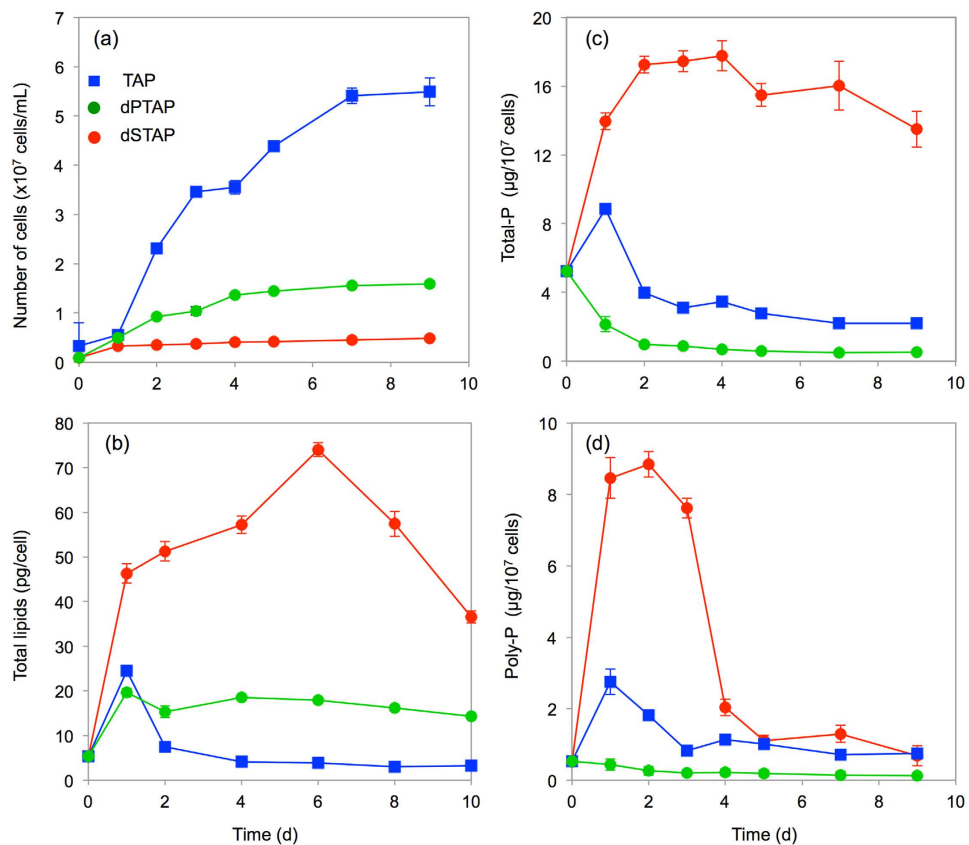


**Figure 2. Lipid and P accumulation is accelerated by S deficiency.** (a) Growth curves of batch cultures of *P. kessleri* in TAP (blue square), dPTAP (green circle), and dSTAP (red circle) medium. (b) Total lipid accumulation in batch cultures in TAP, dPTAP, and dSTAP medium. (c) Total phosphate (total-P) accumulation in batch cultures in TAP, dPTAP, and dSTAP medium. (d) Poly-P accumulation in batch cultures in TAP, dPTAP, and dSTAP medium. Values are means  $\pm$  standard deviation (S.D.) of four independent assays from the same batch culture.

**P is present in DBs under S-depleted conditions.** To determine the elemental profiles of the DBs, we performed EDX analysis using STEM (Fig. 4). Carbon (C) and oxygen (O) were detected as major peaks under all conditions as well as in the background (Fig. 4a,b; Fig. S4). In the dSTAP cultures, a P peak was clearly detected (Fig. 4a); however, a low P peak was detected in the DBs of cells cultured in dPTAP or in the background (Fig. 4c, Fig. S4). A nitrogen (N) peak was detected in cells cultured in the TAP, dSTAP and dPTAP media (Fig. 4a,b; Fig. S4). A copper (Cu) peak was detected in cells cultured in dSTAP (Fig. 4b), which might be contamination from TEM operation. It remains unknown whether there was a larger difference in oxygen amount between  $+/-$ S cells, even if Pi was present.

To assess the presence of elemental P in the DB and non-DB regions of the same cell, an EDX analysis was performed linearly across the section (Fig. 4c,d). Under S-depleted conditions, P was detected in the DB, but not in other non-DB regions of the cytoplasm (Fig. 4c). No P was detected in cells cultured in dPTAP, even in the DB region (Fig. 4d). Considering that poly-P was detected under S-depleted conditions as well as TAP culture (Fig. 2d, Fig. S4), these results indicate that P is present only in the DBs as phosphate; therefore, the DB may be a site of poly-P accumulation. In addition, the DBs maintained their electron density even in the absence of P, indicating that P-free-DBs could be present under phosphorus-depleted conditions.

**Ultrastructural changes of DBs under S-depleted conditions.** P-free-DBs were observed under P-depleted conditions, as mentioned above. Because the poly-P level decreased markedly after culture for 4 d in S-deficient medium (Fig. 2d), we investigated ultrastructural changes during this period. We focused on the ultrastructure of *P. kessleri* cells in the early (2 d), middle (6 d), and late (12 d) periods of culture under S-deficient conditions (Fig. 5). In the early stage of culture, the vacuoles were filled with electron-dense material, within which electron-lucent dot-like structures were observed (Fig. 5a,d). In the middle stage of culture, the electron-lucent region in the DBs had expanded and was frequently located in the center of the DBs (Fig. 5e). In the late stage of culture, the DBs were compressed in the vacuoles (Fig. 5c,f); no dot-like structures were evident. These data suggest ultrastructural variation in the DBs, which may be associated with the presence or absence (hydrolysis) of poly-P.

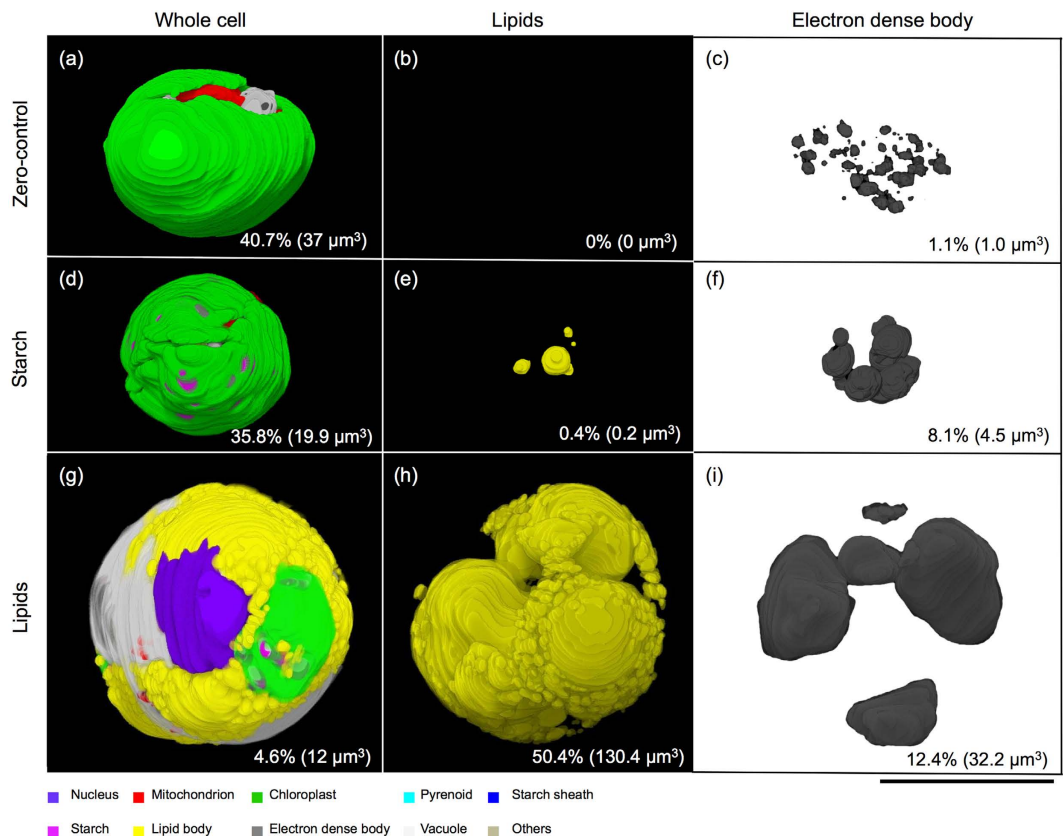


**Figure 3. Lipid hyper-accumulation induces the accumulation of DBs.** (a–c) 3D-TEM images of a zero-control cell from a middle stage culture in TAP medium. (d–f) 3D-TEM images of a starch cell cultured under S-deficient conditions in a 12:12 h light:dark photoperiod (LD). (g–i) 3D-TEM images of a lipid cell cultured under S-deficient conditions in continuous light (LL). Numbers represent means of volumes ( $n = 2$ ) relative to that of the whole cell (%); parentheses enclose the absolute volumes ( $\mu\text{m}^3$ ) of chloroplasts (a,d,g), lipids (b,e,h) and DBs (c,f,i). All subcellular components are denoted as indicated in the legend. See also Movies S1–S10. Scale bar = 5  $\mu\text{m}$ .

**RNA-Seq analysis of cells grown in S-deficient culture.** To assess the transcriptomic response to the presence and absence of S, we reanalyzed the *Parachlorella* RNA-Seq dataset<sup>35</sup> at the early, middle, and late stages of culture. A heat map showing the  $\log_2$ -fold changes of reads per kilobase of exons per million mapped sequence reads (RPKM) values in the early, middle, and late cultures under S-deficient conditions compared to those in the 2-day-old TAP culture is shown in Fig. 6a.

Among the six representative genes of the phosphate symporter/transporter family (the sodium/phosphate symporter is a  $\text{Na}^+$ -Pi cotransporter, and the proton/phosphate symporter is an  $\text{H}^+$ -Pi cotransporter), three were upregulated markedly during the middle and late stages of culture under S-deficient conditions (Fig. 6a). We also compared the absolute RPKM values (Fig. 6b). Among the phosphate symporter/transporter gene family members, *PTB* (10961\_t; accession no. LC093963) showed RPKM values that were markedly higher than those of the other genes, suggesting that *PTB* is a key phosphate transporter gene in *P. kessleri*. Based on the BLASTP search against the *Parachlorella* genome<sup>35</sup>, *PTB* (10961\_t) is a single copy gene in the genome. It should also be noted that *PTB* transcript levels decreased during the culture period (Fig. 6B), which was consistent with the P-accumulation in the early stage of culture under S-depleted conditions. We observed few changes in the *PkAtp* genes that are related to polyphosphate synthesis (except for *PkAtp3* at the late stage; Fig. 6a). We also found a putative poly-P hydrolysis gene (*PkVSP*; 7942\_t) in the *Parachlorella* genome. Although *PkVSP* was slightly downregulated at the late stage, we observed few changes in transcript levels at the early and middle stages (Fig. 6a).

We also focused on genes related to polyphosphate synthesis/degradation and sulfur metabolism, as the present experiment was performed under S-depleted conditions. Of the 15 genes implicated in starch, cysteine, and methionine metabolism, the majority were induced in response to S deficiency at the middle and late stages of culture (Fig. 6b). Although one copy of *cysteine synthase A* (9045\_t) was downregulated, the other four *cysteine synthase A* genes were highly induced in response to sulfur starvation. The *cysteine synthase A* (5154\_t) gene was upregulated 1425-fold (–S/+S) (Fig. 6a).

## Discussion

We determined the site of poly-P accumulation in *Parachlorella kessleri* cells under stress conditions. First, we compared the distribution of the DBs and poly-P accumulation sites of cells cultured under S-depleted conditions

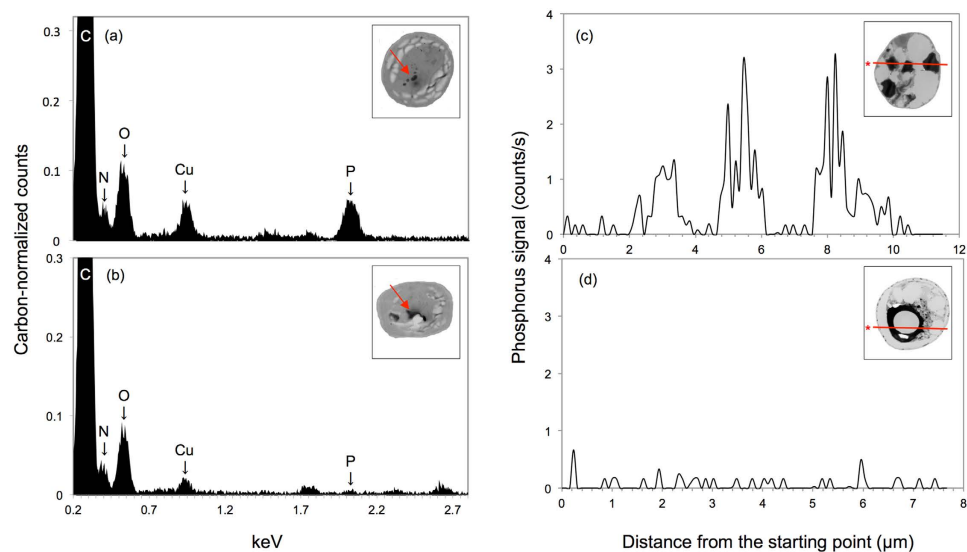


**Figure 4.** DBs in *P. kessleri* cells contain P in dSTAP medium, but not dPTAP medium. EDX spectrometry of the DBs of cells cultured in dSTAP (a) and dPTAP (b) medium. Vertical axis denotes carbon-normalized relative counts and the horizontal axis denotes energy as kilo-electronvolts (keV) (a,b). Intracellular P accumulation in dSTAP medium (c) and dPTAP medium (d) was analyzed linearly by EDX. (Insets) STEM images showing the sites (red arrows or lines) of dot analysis in a and b or line analysis in c and d. Asterisks in c and d show the supplementary data for the EDX analysis of cells cultured in TAP medium and the background.

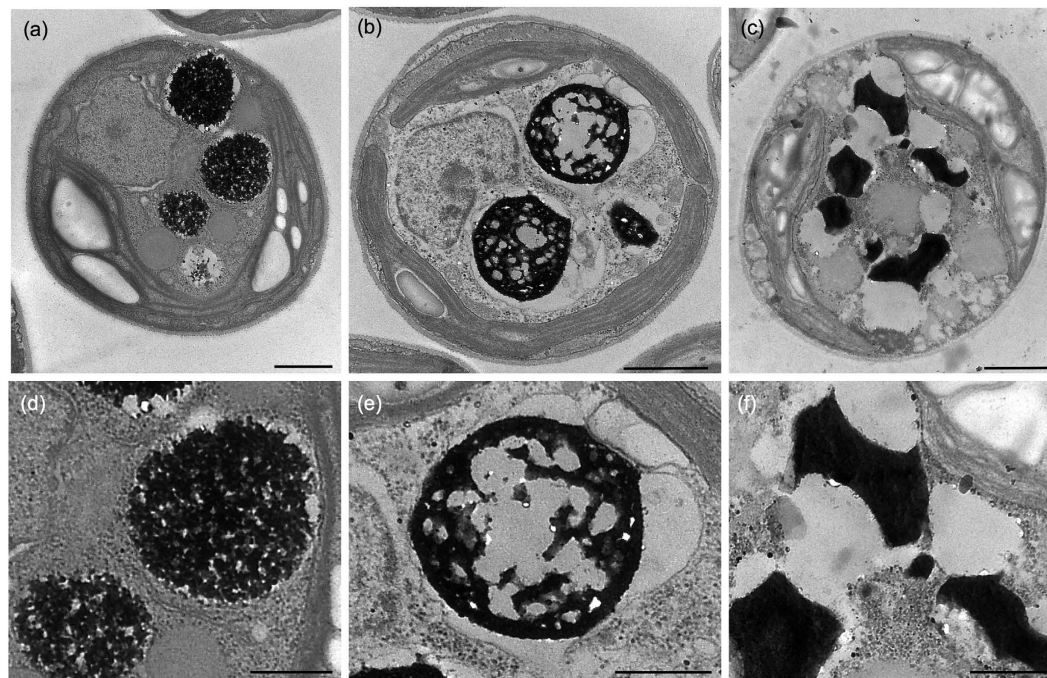


**Figure 5.** Effect of culture age on DB ultrastructure. General ultrastructure of cells from 2-day-old (a), 6-day-old (b), and 12-day-old (c) S-deficient culture. Higher magnification images of DBs in cells from 2-day-old culture (d), 6-day-old culture (e) and 12-day-old culture (f). Bars = 1  $\mu$ m (a–c); 500 nm (d–f).

using fluorescence and transmission microscopy. The subcellular distributional pattern of the DAPI–poly-P complex granules with higher fluorescence was similar to that of the DBs; large granules were localized to the cell periphery while small granules were scattered irregularly (Fig. 1b,c). In addition, serial section analysis showed

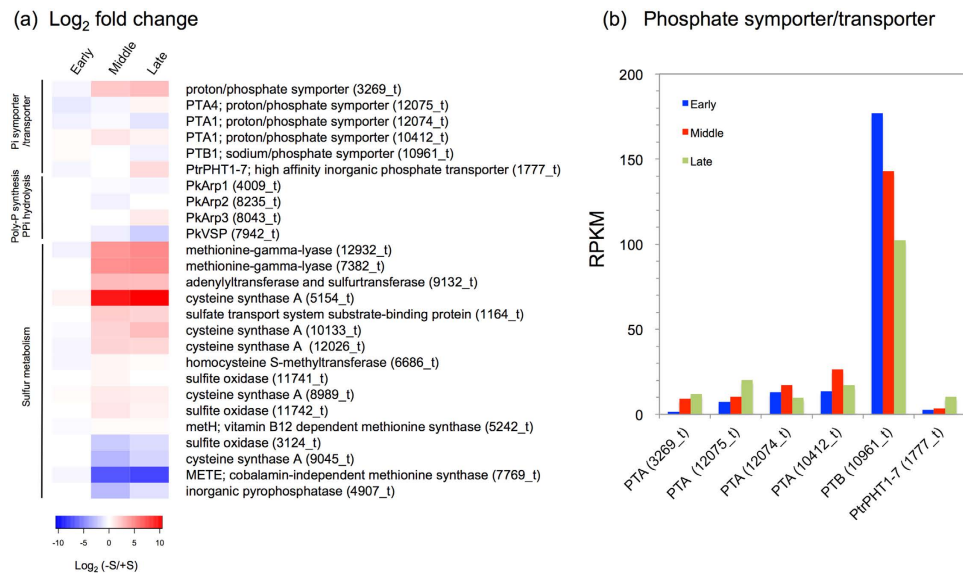


**Figure 6. Transcriptome response to S deficiency by RNA-seq analysis.** (a) Heat map showing the log<sub>2</sub>-scaled fold-changes of RPKM of selected genes (S metabolism, Pi symporter/transporters, poly-P synthesis/PPi hydrolysis) in 2-day-old cultures under S-deprived conditions relative to those under S-replete conditions at the early, middle, and late stages of culture. (b) Absolute values of RPKM for genes related to phosphate symporter/transporters. PTA: proton/phosphate symporter, PTB: sodium/phosphate symporter, PtpPHT1-7: high-affinity inorganic phosphate transporter.

that DBs had affinity for heavy metals but were negative for PAS staining, indicating that DBs contain organic compounds other than sugars and starch. Thus, we infer that the DBs are the sites of poly-P accumulation.

Moreover, we determined the subcellular P accumulation by EDX analysis (Fig. 4, Fig. S4). P was found in the DBs under S-deficient conditions as well as in TAP medium, whereas no P was found in the DBs under P-deficient conditions. The acidocalcisome, a term commonly used to describe an organelle in *C. reinhardtii*, trypanosomatids, and related protists such as *Toxoplasma gondii*<sup>38</sup>, also contains DBs. This organelle contains P in the form of Pi and poly-P as well as calcium (Ca) and other elements such as iron (Fe)<sup>39–41</sup>. In this study, Ca ( $K\alpha = 3.6905$  keV,  $L\alpha = 0.3413$  keV) and Fe ( $K\alpha = 6.3996$  keV,  $L\alpha = 0.7048$  keV), major metal elements of acidocalcisomes, were not detected under any of the culture conditions tested (see Fig. S5), indicating that the DBs detected in *P. kessleri* may be different from acidocalcisomes.

We also examined P accumulation in the non-DB region by linear EDX analysis of cell sections (Fig. 5). P was found only in the DBs in cells cultured in dSTAP medium, and no signal was detected in the DB or non-DB regions in cells cultured under phosphorus-deficient conditions. Based on the EDX analysis and Pi assay data (Fig. 2d), we infer that P is incorporated rapidly into S-depleted cells, and accumulated as poly-P into the DBs, indicating that DBs are sites which serve as Pi reservoirs in *P. kessleri*. However, the nature of the interaction of poly-P with electron dense materials remains to be elucidated. Based on the 3D-TEM data, lipid accumulation may be correlated with increasing DB volume. Pi and lipid accumulation may be a response to S-deficiency stress, the effect of which was enhanced by continuous light. However, the metabolic connection between poly-P and lipid accumulation remains unclear.

Growth of *P. kessleri* was inhibited markedly in dSTAP. Marked lipid accumulation occurs concurrently under conditions of S deficiency. This is consistent with previous reports that lipid levels in *Parachlorella* and *Chlorella* species increased under conditions of S deficiency<sup>32,33</sup>. P-depleted medium also inhibited cell growth, but to a lesser degree than S deficiency (Fig. 2). Our data also suggest that P-deficient cells accumulate lower total lipid levels.

Total-P accumulation increased markedly during the early stage of culture under S-depleted conditions (Fig. 2). With regard to the ratio of the amounts of poly-P to total-P, 43% of incorporated Pi was transformed into poly-P as a storage substance by the end of the early stage (3-day-old culture) (Fig. S3). After culture for 4 d, the poly-P level decreased markedly; however, the total-P level remained roughly constant (Fig. 2). This discrepancy between the poly-P and total-P levels may be explained by hydrolysis of long-chain poly-P in the DB into Pi during the middle and later stages ( $\geq 4$  d) of culture.

Poly-P functions as a protein-protective chaperone for adaptation to stress<sup>42,43</sup>. In this study, total-P and poly-P accumulation accelerated during the early stage of culture under S-deficient conditions. Mutants of *Escherichia coli* that fail to synthesize polyphosphate kinase (PPK) and lack long-chain poly-P fail to survive in the stationary phase and lose their resistance to stresses<sup>44,45</sup>. In *Trypanosoma cruzi*, the concentration of poly-P changes drastically during growth and differentiation. In addition, a response to stress was reported in the halotolerant alga *Dunaliella salina*<sup>46</sup>. Therefore, Pi and poly-P accumulation in *P. kessleri* under S-deficient conditions may also be due to the stress response under S-deficient conditions. Based on the ultrastructural findings and physiological data, we infer that poly-P accumulates in DBs, which function as reservoirs during the early stage of culture.

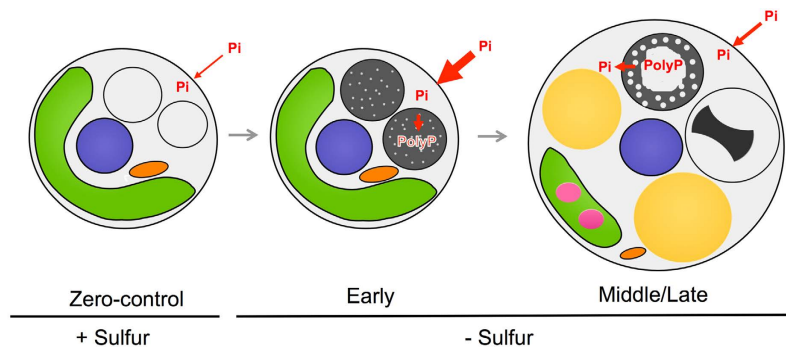


**Figure 7. Schematic illustration of proposed dynamics of Pi and DB ultrastructure in S-deficient culture.** In the S-replete condition, few dense bodies are observed in vacuoles. In the early stage of culture under S deprivation, transportation and accumulation of phosphate (Pi) is accelerated and incorporated into DBs as poly-P. At this stage, the DBs contain electron-opaque materials with small dot-like electron-lucent structures. In the middle/late stage under S deprivation, the electron-lucent regions are expanded, the density of the DBs decreases, and poly-P undergoes partial hydrolysis to Pi. In the late stage, the DBs are highly compressed and Pi may be released to the cytosol and so be absent from the DBs. Arrows indicate the flow of Pi. The thickness of the arrows represents the transcriptomic data. Green, chloroplast; purple, nucleus; magenta, starch; yellow, lipid bodies; gray/black, DB; orange, mitochondria.

To examine the transcriptomic response of genes of interest, we reanalyzed the *Parachlorella* RNA-Seq dataset<sup>35</sup> at the early, middle, and late stages of culture under S-depleted and -replete conditions. Because the present experiment was performed under S-depleted conditions, we also focused on genes related to sulfur metabolism. The vast majority of genes associated with Pi and S metabolism were upregulated in the middle and late stages of culture (Fig. 6). Notably, *PAT1* (*proton/phosphate symporter 1*, 3269\_t), *PAT4*, and *cysteine synthase A* (5154\_t) were highly upregulated in the middle and later stages. The present data on S acquisition and assimilation to cysteine are consistent with a previous study in *Chlamydomonas*<sup>47</sup>.

We could not find *PPK* (polyphosphate kinase) and *PPX* (exopolyphosphatase) homologs in the *Parachlorella* genome<sup>35</sup>. We searched for other candidates of poly-P synthesis/degrading genes in the genome and found a homolog of *Arp* (a gene for actin-related protein): *PkArp1* (4009\_t), *PkArp2* (8235\_t), and *PkArp3* (8043\_t). The *Arp* complex is an enzyme that can polymerize an actin-like filament concurrent with its synthesis of a poly-P chain<sup>48</sup>. We also found a homolog of *VSP* (a vacuolar soluble pyrophosphatase gene), which is a putative gene for poly-P and pyrophosphate hydrolysis<sup>49</sup>. We observed few changes in expression levels of *PkArps* and *PkVSP* under the S-deprivation condition, except in the late stage (Fig. 6a). This result may suggest that poly-P accumulation under S-deprivation is more affected by luxury Pi uptake than by poly-P synthesis/degradation. Further physiological experiments are needed to confirm this conclusion.

Although the ultrastructure of the DBs in *C. pyrenoidosa* has been reported<sup>22</sup>, the ultrastructural changes of the DBs in *Chlorella* species over time remained largely unknown. Based on our findings, we propose the following model of dynamics of poly-P and ultrastructural changes of the DB under S-deficient conditions (Fig. 7). In the early stage of culture, poly-P is accumulated rapidly in the DBs. This is supported by the RNA-Seq data; transcript levels of *PTB*, which encodes a key Pi transporter, decreased during the culture period (Fig. 6b).

The electron-lucent regions in the DBs expanded in cells at the middle stage of culture. In cells during the late stage of culture, the DBs were compressed and localized to the vacuole (Fig. 7). The compressed DBs were electron-opaque and lacked the dot-like structures present in the early and middle stages. Intriguingly, the ultrastructure of the compressed DBs was similar to that of the DBs in cells cultured under P-deficient conditions (Fig. S6), suggesting them to be of the same type as the Pi-free-DBs present in cells in the later stage of culture under S-deficient conditions. Taken together, our findings show that DBs in *P. kessleri* are sites of accumulation of poly-P and that DB ultrastructure varies considerably according to the presence or absence of poly-P.

In this study, our data indicate that P accumulation increased markedly under sulfur-depleted conditions, and that DBs are a polyphosphate accumulation site in the green alga *Parachlorella kessleri*. In addition, considerable ultrastructural variation was observed in DBs according to the amount of P. The TEM observations revealed marked ultrastructural variations in the DBs with or without poly-P, as well as hyper-accumulation of lipids. Based on our findings, we propose that the DBs are a site of poly-P accumulation during the early stage of culture under S-depleted conditions. Because *P. kessleri* achieves high poly-P content, as well as high biomass and lipid production, this species has potential as a phosphate accumulating organism.

## Methods

**Strains and growth media.** *Parachlorella kessleri* strain NIES-2152 was obtained from the Microbial Culture Collection, National Institute for Environmental Studies, Tsukuba, Japan (<http://mcc.nies.go.jp/>). Precultures were grown for 4 d in a test tube (TEST 30 NP; IWAKI, Tokyo, Japan) in 30 mL of Tris-acetate-phosphate (TAP) medium (Table S1) at 23 °C under a 12 h light (L):12 h dark (D) cycle. The culture was incubated under a photon flux of  $\sim 100 \mu\text{mol m}^{-2} \text{s}^{-1}$  with agitation using a magnetic stirrer (MGM-66, Shibata, Tokyo, Japan) at approximately 100 rpm. For nutrient limitation, sulfur ( $\text{SO}_4^{2-}$ )-deficient TAP (dSTAP; Table S2) and phosphorus-deficient TAP (dPTAP; Table S3) media were used.



**Transmission electron microscopy.** Five-day-old cultures grown in dSTAP (LL) were fixed with 2.5% glutaraldehyde (GA) for 2 h at room temperature (r.t.). To permeate GA, the cell suspension was microwaved for 20 s on ice at the beginning of the fixation. The cells were washed four times with 0.1 M sodium cacodylate buffer (pH 7.2). After centrifugation and removal of the supernatant, the pellet was post-fixed with 1% osmium tetroxide for 2 h at r.t. Dehydration, embedding, and uranyl acetate-lead citrate staining methods followed the procedures described by Wayama *et al.*<sup>50</sup>. For silver-protein staining, sections were treated with periodic acid-thiocarbohydrazide and then stained with silver proteinate<sup>37</sup>.

**Energy dispersive X-ray spectroscopy.** Six-day-old cultures grown under LD conditions were fixed with 2.5% glutaraldehyde. Dehydration and embedding methods followed the procedures described by Wayama *et al.*<sup>50</sup>. Ultrathin sections were cut on a Reichert Ultracut S ultramicrotome (Leica, Vienna, Austria) using a diamond knife, mounted on a copper grid and observed without staining using an HT7700 electron microscope (Hitachi, Tokyo, Japan) operating at 100 kV. The elemental composition of DBs was determined by energy-dispersive X-ray spectroscopy (EDS; X-Max80, Horiba, Kyoto, Japan). The measurement points or lines are indicated in the dark-field STEM images.

**Poly-P detection by staining with 4',6-diamidino-2-phenylindole (DAPI).** Poly-P can be stained by high concentrations of DAPI. The peak emission wavelength of the resulting DAPI-poly-P complex is ~525 nm; *i.e.*, a yellow or greenish-yellow color. For poly-P observations, cells were fixed with 1% GA for 5 min at r.t. and washed with phosphate-buffered saline (pH 7.4) containing 0.1% Triton X-100. Cell suspensions were stained with DAPI at a final concentration of 100 µg/mL. After incubation for 1 h at r.t., cells were observed using a BX-60 fluorescence microscope (Olympus, Tokyo, Japan) equipped with a DP70 CCD camera (Olympus, Tokyo, Japan). For poly-P detection, UV excitation was used and emission at >420 nm was detected using a U-MWU filter cube.

**Growth, lipids, and total phosphate (total-P) and poly-P assays.** Cell numbers were determined using a particle counter (CDA-1000, SYSMEX, Kobe, Japan). The lipid assay described by Takeshita *et al.* was used<sup>32</sup>. For a total-P assay, 10 mL of culture were sampled, centrifuged at  $2,500 \times g$  for 5 min, and the pelleted cells were collected. The pellet was resuspended in distilled water (DW) and washed by centrifugation at  $2,500 \times g$  for 5 min. The pellet was resuspended in 1 mL of DW, and the cells were disrupted by vortexing with glass beads for 15 min at 4 °C. For hydrolysis to orthophosphate, 200 µL of 4% (w/v) potassium persulfate were added to the sample, which was then autoclaved at 121 °C for 30 min. The lysate was subjected to a molybdenum blue assay (see below).

For a poly-P assay, 10 mL of culture were sampled, centrifuged at  $2,500 \times g$  for 5 min, and the pelleted cells were collected. The pellet was resuspended in 1 mL of 5% sodium hypochlorite, and the cells were disrupted by vortexing with glass beads for 15 min at 4 °C. After centrifugation at  $14,000 \times g$  for 3 min, the supernatant was removed, and then the pellet was resuspended in 1 mL of 5% sodium hypochlorite, centrifuged at  $14,000 \times g$  for 3 min, and the supernatant was again removed. Next, the pellet was resuspended in 100 µL of DW, followed by incubation for 5 min at r.t. and centrifugation at  $14,000 \times g$  for 3 min; the supernatant was then decanted. Again, the pellet was resuspended in 100 µL of DW, followed by incubation for 5 min at r.t. and centrifugation at  $14,000 \times g$  for 3 min; the supernatant was then collected. The retrieved supernatant (200 µL) containing poly-P was precipitated with 90% ethanol (final conc.), centrifuged at  $14,000 \times g$  for 10 min, and the supernatant removed. The poly-P pellet was then dissolved in 50 µL of DW. For hydrolysis to orthophosphate, 100 µL of 4% (w/v) potassium persulfate were added to the poly-P solution, followed by autoclaving at 121 °C for 30 min and subjecting to a molybdenum blue assay (see below).

Orthophosphate (Pi) was assayed by the molybdenum blue method in a 96-well microplate (IWAKI, Tokyo, Japan). A diluted phosphate sample (200 µL) was pipetted into the wells, and 8 µL of ammonium molybdate tetrahydrate solution [1.2% (w/v) with 4.8 mg potassium antimonyl tartrate sesquihydrate and 16 mL sulfuric acid per 100 mL DW] and 2 µL of 7.2% (w/v) L-ascorbic acid solution were added, and the solution mixed. After incubation for 20 min at r.t. in the dark, absorbance at 880 nm was read using a microplate reader (Viento nano; BioTek Japan, Tokyo, Japan). Phosphate Ion Standard Solution (Wako Pure Chemical Industries, Osaka, Japan) was used for the standard curve, the linearity range of which was 0 to 2 mg NaH<sub>2</sub>PO<sub>4</sub>/L.

**Three-dimensional transmission electron microscopy (3D-TEM) analysis.** For 3D-TEM analysis, we reconstructed 3D images of a 4-day-old cell grown in sulfur (S)-replete medium (TAP, no-stress condition) (zero-control cell), a 6-day-old cell grown in S-deficient medium (dSTAP) under a 12:12 h light:dark photoperiod (LD) (starch cell), and a 6-day-old cell cultured in S-deficient medium (dSTAP) under continuous light (LL) (lipid cell). The detailed procedures for TEM and 3D reconstruction are described in Wayama *et al.*<sup>50</sup>, with the exception of the modifications described below. Digital stacked images were displayed on a tablet device (iPad; Apple Inc., CA) and the contours of each subcellular element were traced manually in color using Procreate (ver. 2.0.2). The traced images were converted into digital images (JPG format), and 3D reconstructions were performed using the TRI/3D SRF III software (Ratoc System Engineering, Co., Ltd., Tokyo, Japan). Each subcellular volume was calculated from voxels using the TRI/3D SRF III software. Values are the means of two representative cells in each growth phase.

**RNA-Seq analysis.** To focus on the transcriptomic responses of genes associated with Pi and S metabolism, we reanalyzed the *Parachlorella* RNA-Seq dataset<sup>35</sup>. The methods for total RNA extraction, mRNA purification, and RNA sequencing were described previously<sup>35</sup>. Briefly, total RNA was extracted from cultures with or without S in the early (2-day-old cells) and late (4–5-day-old cells) logarithmic and stationary phases (7–8-day-old cells). The mRNA sequencing libraries of *P. kessleri* NIES-2152 were constructed using the Ion Total RNA-Seq Kit v2 (Life Technologies, Carlsbad, CA, USA), and the libraries were sequenced using an Ion PGM Sequencer (Life

Technologies). The heatmap was generated using the heatmap2 function in Gplots package v. 2.16.0 in R statistical software v. 3.1.0 (<http://www.R-project.org/>).

## References

- Smil, V. Phosphorus in the environment: natural flows and human interferences. *Annu. Rev. Energy Environ.* **25**, 53–88 (2000).
- Koppelaar, R. H. E. M. & Weikard, H. P. Assessing phosphate rock depletion and phosphorus recycling options. *Glob. Environ. Chang.* **23**, 1454–1466 (2013).
- Cordell, D. & White, S. Peak phosphorus: clarifying the key issues of a vigorous debate about long-term phosphorus security. *Sustainability* **3**, 2027–2049 (2011).
- Powell, N., Shilton, A. N., Pratt, S. & Chisti, Y. Factors influencing luxury uptake of phosphorus by microalgae in waste stabilization ponds. *Environ. Sci. Technol.* **42**, 5958–5962 (2008).
- McMahon, K. D. & Read, E. K. Microbial contributions to phosphorus cycling in eutrophic lakes and wastewater. *Annu. Rev. Microbiol.* **67**, 199–219 (2013).
- Solovchenko, A., Verschoor, A. M., Jablonowski, N. D. & Nedbal, L. Phosphorus from wastewater to crops: An alternative path involving microalgae. *Biotechnol. Adv.* in press (2016), doi:10.1016/j.biotechadv.2016.01.002.
- Kornberg, A., Rao, N. N. & Ault-Riché, D. Inorganic polyphosphate: a molecule of many functions. *Annu. Rev. Biochem.* **68**, 89–125 (1999).
- Rao, N. N., Gómez-García, M. R. & Kornberg, A. Inorganic polyphosphate: essential for growth and survival. *Annu. Rev. Biochem.* **78**, 605–647 (2009).
- Seufferheld, M. *et al.* Identification of organelles in bacteria similar to acidocalcisomes of unicellular eukaryotes. *J. Biol. Chem.* **278**, 29971–29978 (2003).
- Pallerla, S. R. *et al.* Formation of volutin granules in *Corynebacterium glutamicum*. *FEMS Microbiol. Lett.* **243**, 133–140 (2005).
- Brock, J., Rhiel, E., Beutler, M., Salman, V. & Schulz-Vogt, H. N. Unusual polyphosphate inclusions observed in a marine *Beggiatoa* strain. *Antonie Van Leeuwenhoek* **101**, 347–357 (2012).
- Marchesini, N., Luo, S., Rodrigues, C. O., Moreno, S. N. & Docampo, R. Acidocalcisomes and a vacuolar H<sup>+</sup>-pyrophosphatase in malaria parasites. *Biochem. J.* **347** Pt 1, 243–253 (2000).
- Docampo, R., Ulrich, P. & Moreno, S. N. J. Evolution of acidocalcisomes and their role in polyphosphate storage and osmoregulation in eukaryotic microbes. *Philos. Trans. R. Soc. Lond. B. Biol. Sci.* **365**, 775–784 (2010).
- Marchesini, N., Ruiz, F. A., Vieira, M. & Docampo, R. Acidocalcisomes are functionally linked to the contractile vacuole of *Dictyostelium discoideum*. *J. Biol. Chem.* **277**, 8146–8153 (2002).
- Breus, N. A., Ryazanova, L. P., Dmitriev, V. V., Kulakovskaya, T. V. & Kulaev, I. S. Accumulation of phosphate and polyphosphate by *Cryptococcus humicola* and *Saccharomyces cerevisiae* in the absence of nitrogen. *FEMS Yeast Res.* **12**, 617–624 (2012).
- Vitová, M., Hendrychová, J., Cepák, V. & Zachleder, V. Visualization of DNA-containing structures in various species of Chlorophyta, Rhodophyta and Cyanophyta using SYBR Green I dye. *Folia Microbiol.* **50**, 333–340 (2005).
- Ramos, I. *et al.* Acidocalcisomes as calcium- and polyphosphate-storage compartments during embryogenesis of the insect *Rhodnius prolixus* Stahl. *PLoS One* **6**, e27276 (2011).
- Yagisawa, F., Nishida, K., Kuroiwa, H., Nagata, T. & Kuroiwa, T. Identification and mitotic partitioning strategies of vacuoles in the unicellular red alga *Cyanidioschyzon merolae*. *Planta* **226**, 1017–1029 (2007).
- Yagisawa, F. *et al.* Identification of novel proteins in isolated polyphosphate vacuoles in the primitive red alga *Cyanidioschyzon merolae*. *Plant J.* **60**, 882–893 (2009).
- Komine, Y., Eggink, L. L., Park, H. & Hooper, J. K. Vacuolar granules in *Chlamydomonas reinhardtii*: polyphosphate and a 70-kDa polypeptide as major components. *Planta* **210**, 897–905 (2000).
- Aksoy, M., Pootakham, W. & Grossman, A. R. Critical function of a *Chlamydomonas reinhardtii* putative polyphosphate polymerase subunit during nutrient deprivation. *Plant Cell* **26**, 4214–4229 (2014).
- Peverly, J. H. & Adamec, J. Association of potassium and some other monovalent cations with occurrence of polyphosphate bodies in *Chlorella pyrenoidosa*. *Plant Physiol.* **62**, 120–126 (1978).
- Meza, B., De-Bashan, L. E., Hernandez, J.-P. & Bashan, Y. Accumulation of intra-cellular polyphosphate in *Chlorella vulgaris* cells is related to indole-3-acetic acid produced by *Azospirillum brasilense*. *Res. Microbiol.* **166**, 399–407 (2015).
- Aschar-Sobbi, R. *et al.* High sensitivity, quantitative measurements of polyphosphate using a new DAPI-based approach. *J. Fluorescence* **18**, 859–866 (2008).
- Gomes, F. M. *et al.* New insights into the *in situ* microscopic visualization and quantification of inorganic polyphosphate stores by 4',6-diamidino-2-phenylindole (DAPI)-staining. *Eur. J. Histochem.* **57**, e34 (2013).
- Kulakova, A. N. *et al.* Direct quantification of inorganic polyphosphate in microbial cells using 4',6-diamidino-2-phenylindole (DAPI). *Environ. Sci. Technol.* **45**, 7799–7803 (2011).
- Vitová, M., Bišová, K., Kawano, S. & Zachleder, V. Accumulation of energy reserves in algae: From cell cycles to biotechnological applications. *Biotechnol. Adv.* **33**, 1204–1218 (2015).
- Brányiková, I. *et al.* Microalgae—novel highly efficient starch producers. *Biotechnol. Bioeng.* **108**, 766–776 (2011).
- Ault-Riché, D., Fraley, C. D., Tzeng, C. M. & Kornberg, A. Novel assay reveals multiple pathways regulating stress-induced accumulations of inorganic polyphosphate in *Escherichia coli*. *J. Bacteriol.* **180**, 1841–1847 (1998).
- Ruiz, F. A., Rodrigues, C. O. & Docampo, R. Rapid changes in polyphosphate content within acidocalcisomes in response to cell growth, differentiation, and environmental stress in *Trypanosoma cruzi*. *J. Biol. Chem.* **276**, 26114–26121 (2001).
- Krienitz, L. *et al.* Phylogenetic relationship of *Chlorella* and *Parachlorella* gen. nov. (Chlorophyta, Trebouxiophyceae). *Phycologia* **43**, 529–542 (2004).
- Takeshita, T. *et al.* Starch and lipid accumulation in eight strains of six *Chlorella* species under comparatively high light intensity and aeration culture conditions. *Bioresour. Technol.* **158**, 127–134 (2014).
- Mizuno, Y. *et al.* Sequential accumulation of starch and lipid induced by sulfur deficiency in *Chlorella* and *Parachlorella* species. *Bioresour. Technol.* **129**, 150–155 (2013).
- Li, X. *et al.* The microalga *Parachlorella kessleri*—a novel highly efficient lipid producer. *Biotechnol. Bioeng.* **110**, 97–107 (2013).
- Ota, S. *et al.* Highly efficient lipid production in the green alga *Parachlorella kessleri*: draft genome and transcriptome endorsed by whole-cell 3D ultrastructure. *Biotechnol. Biofuels* **9**, 13 (2016).
- Reynolds, E. S. The use of lead citrate at high pH as an electron-opaque stain in electron microscopy. *J. Cell Biol.* **17**, 208–212 (1963).
- Courtroy, R. & Simar, L. J. Importance of controls for the demonstration of carbohydrates in electron microscopy with the silver methanamine or the thiocarbonylhydrazide-silver proteinate methods. *J. Microsc.* **100**, 199–211 (1974).
- Docampo, R., de Souza, W., Miranda, K., Rohloff, P. & Moreno, S. N. J. Acidocalcisomes - conserved from bacteria to man. *Nat. Rev. Microbiol.* **3**, 251–261 (2005).
- Docampo, R. & Moreno, S. N. Acidocalcisome: A novel Ca<sup>2+</sup> storage compartment in trypanosomatids and apicomplexan parasites. *Parasitol. Today* **15**, 443–448 (1999).
- Ruiz, F. A., Marchesini, N., Seufferheld, M., Govindjee & Docampo, R. The polyphosphate bodies of *Chlamydomonas reinhardtii* possess a proton-pumping pyrophosphatase and are similar to acidocalcisomes. *J. Biol. Chem.* **276**, 46196–46203 (2001).

41. Huang, G. *et al.* Adaptor protein-3 (AP-3) complex mediates the biogenesis of acidocalcisomes and is essential for growth and virulence of *Trypanosoma brucei*. *J. Biol. Chem.* **286**, 36619–36630 (2011).
42. Gray, M. J. *et al.* Polyphosphate is a primordial chaperone. *Mol. Cell* **53**, 689–699 (2014).
43. Gray, M. J. & Jakob, U. Oxidative stress protection by polyphosphate—new roles for an old player. *Curr. Opin. Microbiol.* **24**, 1–6 (2015).
44. Croke, E., Akiyama, M., Rao, N. N. & Kornberg, A. Genetically altered levels of inorganic polyphosphate in *Escherichia coli*. *J. Biol. Chem.* **269**, 6290–6295 (1994).
45. Rao, N. N. & Kornberg, A. Inorganic polyphosphate supports resistance and survival of stationary-phase *Escherichia coli*. *J. Bacteriol.* **178**, 1394–1400 (1996).
46. Pick, U. & Weiss, M. Polyphosphate hydrolysis within acidic vacuoles in response to amine-induced alkaline stress in the halotolerant alga *Dunaliella salina*. *Plant Physiol.* **97**, 1234–1240 (1991).
47. González-Ballester, D. *et al.* RNA-seq analysis of sulfur-deprived *Chlamydomonas* cells reveals aspects of acclimation critical for cell survival. *Plant Cell* **22**, 2058–2084 (2010).
48. Gómez-García, M. R. & Kornberg, A. Formation of an actin-like filament concurrent with the enzymatic synthesis of inorganic polyphosphate. *Proc. Natl. Acad. Sci. USA* **101**, 15876–15880 (2004).
49. Lander, N., Cordeiro, C., Huang, G. & Docampo, R. Polyphosphate and acidocalcisomes. *Biochem. Soc. Trans.* **44**, 1–6 (2016).
50. Wayama, M. *et al.* Three-dimensional ultrastructural study of oil and astaxanthin accumulation during encystment in the green alga *Haematococcus pluvialis*. *PLoS One* **8**, e53618 (2013).

## Acknowledgements

We thank Yuko Yoshizawa, Rika Shinohara, Yukiko Kudo, and Minako Miki (University of Tokyo) for their technical assistance with this research. We thank Dr. Nobuhito Nango (Ratoc System Engineering Japan) for helpful discussion and technical assistance with 3D-TEM analysis. This research was supported with funding provided by the Japan Science and Technology Agency (JST) in the CREST program (to S.K.).

## Author Contributions

S.K. conceived the project and supervised this study. M.Y., A.H. and M.K. performed TEM and EDX analysis. T.Y., K.O. and M.H. performed RNA-seq analysis. M.Y. and T.T. performed lipid assay and S.O. measured number of cells, poly-P and total-P contents. S.O. analyzed the resulting data. S.O. and S.K. wrote the manuscript. T.Y., T.T., K.B. and V.Z. assisted with the manuscript writing and participated in detailed discussion of study design.

## Additional Information

**Accession Codes:** The sequencing data used in the present RNA-seq analysis have been deposited in the DDBJ database under accession numbers: LC093959 (12075\_t), LC093960 (12074\_t), LC093961 (3269\_t), LC093962 (10412\_t), LC093963 (10961\_t), LC093964 (1777\_t), LC093965 (12932\_t), LC093966 (7382\_t), LC093967 (9132\_t), LC093968 (5154\_t), LC093969 (1164\_t), LC093970 (10133\_t), LC093971 (12026\_t), LC093972 (6686\_t), LC093973 (11741\_t), LC093974 (8989\_t), LC093975 (11742\_t), LC093976 (5242\_t), LC093977 (3124\_t), LC093978 (9045\_t), LC093979 (7769\_t), LC128310 (4009\_t), LC128311 (8235\_t), LC128312 (8043\_t), LC128419 (7942\_t).

**Supplementary information** accompanies this paper at <http://www.nature.com/srep>

**Competing financial interests:** The authors declare no competing financial interests.

**How to cite this article:** Ota, S. *et al.* Deciphering the relationship among phosphate dynamics, electron-dense body and lipid accumulation in the green alga *Parachlorella kessleri*. *Sci. Rep.* **6**, 25731; doi: 10.1038/srep25731 (2016).



This work is licensed under a Creative Commons Attribution 4.0 International License. The images or other third party material in this article are included in the article's Creative Commons license, unless indicated otherwise in the credit line; if the material is not included under the Creative Commons license, users will need to obtain permission from the license holder to reproduce the material. To view a copy of this license, visit <http://creativecommons.org/licenses/by/4.0/>